On the effects of limited spectral resolution in third-generation wave models

I. V. Lavrenov and J. R. A. Onvlee

Technical reports; TR-156
Technische rapporten; TR-156

De Bilt, 1993

On the effects of limited spectral resolution in third-generation wave models

I.V. Lavrenov[1,2] and J.R.A. Onvlee[3]
1 - State Oceanographic Institute of Russia, St. Petersburg Dept.
2 - visitor at KNMI, De Bilt, The Netherlands
3 - KNMI, De Bilt, The Netherlands

Abstract:

In spectral wave models, wave propagation suffers from the so-called garden-sprinkler effect: due to the treatment of spectral bands of finite width as individual (continuous) wave components, most of the energy of the propagating wave becomes concentrated along the main directions recognized by the model. In this paper a method is proposed aiming to diminish the garden sprinkler effect in numerical wave models without paying the penalty of a large increase in computation time. Starting from the energy balance equation, additional terms are derived which correct for the finite width of the angular bands. The correction terms are defined locally, hence knowledge of large-scale quantities is not required for their computation; however, they do contain additional angular and spatial derivatives, the calculation of which may be costly. It is shown that for areas of limited spatial extent the correction terms may be approximated by a simple diffusive operator depending on the scale length of propagation. Inclusion of the angular diffusion term in the WAM propagation scheme leads to a significant decrease of the garden sprinkler effect in this model. The simplified correction term requires little computation time and can easily be implemented in spectral wind wave models.

1 Introduction

Present state-of-the-art wave models are formulated in terms of a wave energy spectrum discretized into a large number of spectral bands. The finite width of these bands introduces non-trivial complications for the computation of wave propagation. Ideally, the energy of a wave disturbance of small initial extent will spread out smoothly over the sea or ocean in the course of time. In most of the presently operational models, however, the spectral resolution is so coarse that the so-called "garden-sprinkler" effect occurs (e.g. [4],[8],[9]): most of the

energy of the propagating wave becomes concentrated along the basic directions of the model which are closest to the direction of wave propagation, while in other directions the wave energy is underestimated. Thus, the limited angular resolution of the model introduces a measure of artificial anisotropy in the spatial distribution of wave height. One consequence of this phenomenon is that the arrival of swell originating from distant storms is often poorly predicted [1,4].

A straightforward way to remove this problem is simply to increase the spectral resolution. This is computationally expensive, however. A second solution to the garden sprinkler problem was derived by Booy and Holthuijsen [4], for wave propagation over a plain surface. Their approach consists of adding two terms to the energy balance equation, which correct for the finite width of the angular and frequency bands. The disadvantage of inclusion of the correction terms of Booij and Holthuijsen in spectral wave propagation schemes is that this requires the solution of a more complex equation than the energy balance equation, with a corresponding increase in computing time.

In the present paper we propose another approach, capable of removing the garden sprinkler effect to a large extent without demanding a significant additional amount of cpu-time. The method adopted here is outlined in section 2. We consider the case of pure swell propagation on the sphere in deep water. For this problem an analytical solution can be derived. Correction terms to the energy balance equation are derived in a manner similar to that of Booij and Holthuijsen. In the case of propagation over an area of limited extent (such as the North Sea), these correction terms can be reduced to a simple angular diffusive operator, which can be implemented in numerical propagation schemes at little computational cost.

In section 3, the proposed solution is applied to the WAM-model [5]. A wave disturbance of prescribed initial shape and spectrum is assumed to propagate through a deep water region of roughly 20 by 20 degrees in extent. The analytical solution of this problem is derived and compared to the results of the standard WAM model and to the modified version including an angular diffusive operator.

2 The angular smoothing technique

The strong influence of the garden sprinkler effect on presently operational spectral wave models (e.g. [1],[4],[8],[9]) is due mainly to the coarseness of the angular resolution adopted (generally 15 or 30 degrees); the discretization of the spectrum into frequency bands plays a less important role. For this reason we will limit ourselves to a discussion of the consequences of describing the spectrum with angular bands of finite width only; but in principle all of the following can be applied to frequency as well.

In the energy balance equation, the evolution of a wave spectrum S($\omega, \beta, \phi, \theta$, t) with respect to frequency ω, propagation direction β (measured here counterclockwise from the parallel), latitude ϕ and longitude θ (on the spherical earth) and time, is described in the form of a differential operator:

$$L(S) = \frac{\partial S}{\partial t} + \frac{1}{\cos\phi}\frac{\partial(\dot{\phi}\cos\phi\, S)}{\partial\phi} + \frac{\partial(\dot{\theta}\, S)}{\partial\theta} + \frac{\partial(\dot{\beta}\, S)}{\partial\beta} = G \qquad (1)$$

G = G($\omega, \beta, \phi, \theta$, t) is the function describing the sources and sinks of wave energy, consisting of wind input, bottom friction, dissipation and non-linear interaction terms. The functions $\dot{\phi}$, $\dot{\theta}$ and $\dot{\beta}$ represent the rates of change of position (ϕ, θ) and direction of propagation β of a wave packet travelling along the ray (a great circle):

$$\dot{\phi} = C_g \sin\beta \;/\; \mathrm{R} \qquad (2)$$

$$\dot{\theta} = C_g \cos\beta \;/(\mathrm{R}\cos\phi) \qquad (3)$$

$$\dot{\beta} = -C_g \tan\phi \cos\beta \;/\; \mathrm{R} \qquad (4)$$

where C_g is the wave group velocity and R is the earth radius.

We will investigate the solution of equation (1) for the case of pure swell propagation, assuming the source term G to be zero: L(S)=0.

2.1 Effects of angular discretization

Numerical solution of the energy balance equation (1) requires the discretization of the continuous wave spectrum in frequency-direction space. Let $S^n(\omega_k, \beta_l)$ be the wave spectral

component at time step n corresponding to frequencies in the range ($\omega_k - 0.5\ \Delta\omega \leq \omega \leq \omega_k + 0.5\ \Delta\omega$) ω_k and directions in the band ($\beta_l - 0.5\ \Delta\beta \leq \beta \leq \beta_l + 0.5\ \Delta\beta$). The mean energy contained in the angular range ($\beta_l - 0.5\ \Delta\beta \leq \beta \leq \beta_l + 0.5\ \Delta\beta$) can be determined by integrating the energy balance equation (1) over the angular band width:

$$\overline{S}(\omega_k, \beta_l) \;=\; \frac{1}{\Delta\beta} \int_{\beta_l - \frac{\Delta\beta}{2}}^{\beta_l + \frac{\Delta\beta}{2}} S\ d\beta \tag{5}$$

The usual way to estimate the integral (5) is to use first-order numerical integration schemes [1-5]. Under the assumption that S is continuous and twice differentiable, a more accurate second-order algorithm can be used. To derive the mean energy in the band ($\beta_l - 0.5\ \Delta\beta \leq \beta \leq \beta_l + 0.5\ \Delta\beta$), quadratic interpolation is applied between three points β_{l-1}, β_l and β_{l+1}. The mean energy value can then be approximated by:

$$\overline{S}(\omega_k, \beta_l) \;=\; \sum_{j=-1}^{1} a_j\ S(\omega_k, \beta_{l+j}) \tag{6}$$

where the interpolation coefficients $a_{-1} = a_1 = 1/24$; $a_o = 11/12$. The mean energy contained within the band therefore does originate not only from the component $S(\omega_k, \beta_l)$, but from neighbouring (in direction space) components as well.

In a similar manner the energy balance equation can be adapted to incorporate the effects of a finite angular resolution $\Delta\beta$, by applying to it the integral operator:

$$\frac{1}{\Delta\beta} \int_{\beta_l - \Delta\beta/2}^{\beta_l + \Delta\beta/2} L(S)\ d\beta \tag{7}$$

By using the definition of mean energy (6) and by applying the following expansion, which is valid for small values of $|\ \Delta\beta\ | < 1$:

$$\cos\beta_{l\pm1} \;=\; \cos(\beta_l \pm \Delta\beta) \;=\; \cos\beta_l\,(1 - (\Delta\beta)^2/2) \mp \sin\beta_l\ \Delta\beta + O((\Delta\beta)^3)$$

$$\sin\beta_{l\pm1} \;=\; \sin(\beta_l \pm \Delta\beta) \;=\; \sin\beta_l\,(1 - (\Delta\beta)^2/2) \pm \cos\beta_l\ \Delta\beta + O((\Delta\beta)^3)$$

it can be shown that:

$$\begin{aligned} &\frac{\partial\overline{S}}{\partial t} + \frac{1}{\cos\phi}\frac{\partial}{\partial\phi}(\dot{\phi}\,(1 + \epsilon/2)\cos\phi\ \overline{S}) + \\ &\quad + \frac{\partial}{\partial\theta}(\dot{\theta}\,(1 + \epsilon/2)\,\overline{S}) + \frac{\partial}{\partial\beta}(\dot{\beta}\,(1 + \epsilon)\,\overline{S}) + \\ &+ \frac{\epsilon C_g}{R}\frac{\partial}{\partial\beta}\{\frac{\partial(\overline{S}\cos\beta)}{\partial\phi} - \frac{1}{\cos\phi}\frac{\partial(\overline{S}\sin\beta)}{\partial\theta} + \frac{1}{2}\tan\phi\cos\beta\frac{\partial^2\overline{S}}{\partial\beta^2}\} + O(\epsilon^2) \;=\; 0 \end{aligned} \tag{8}$$

where $\epsilon = (\Delta\beta)^2/12 \ll 1$.

The first four terms in eq.(8) are similar in nature to the terms on the left-hand side of the original energy balance equation (1). In addition they contain a correction term of order ϵ, which describes changes in the velocity of spectral components due to the angular discretization. Since in general ϵ is small (for the standard WAM model with 12 directions $\epsilon \approx 2\%$), the contribution of this term to the factor $(1 + \epsilon/2)$ is negligible. The same holds for the sixth term on the left-hand side of (8). It is the fifth term in (8) which provides the corrections required to represent the effects of finite angular resolution on the evolution of the wave spectrum. This term contains second-order spatial and angular derivatives. It is proportional to ϵ (in other words, to $(\Delta\beta)^2$), to the group velocity C_g and the radius of the Earth R. The fifth term itself consists of three parts. The first two contributions are determined by spatial and angular inhomogeneities of the wave field; the third part describes the wave variance due to changes in wave propagation angle β as the wave travels along a great circle.

The fifth term in eq.(8) is comparable to a similar term derived in an analogous manner by Booij and Holthuijsen [4], for the case of wave propagation over a plain surface. The correction term given by Booij and Holthuijsen depends on a quantity which they term "wave age", which is not defined locally. The main advantage of the angular correction term applied here is that it is defined purely locally for a spherical surface. For a plain surface, a correction term for finite angular resolution can be derived in a manner analogous to eq.(8):

$$\frac{\partial \overline{S}}{\partial t} + C_{gx}\frac{\partial \overline{S}}{\partial x} + C_{gy}\frac{\partial \overline{S}}{\partial y} + \epsilon\, C_g \frac{\partial}{\partial \beta}\{\frac{\partial(\overline{S}\cos\beta)}{\partial y} - \frac{\partial(\overline{S}\sin\beta)}{\partial x}\} = 0 \qquad (9)$$

where $C_{gx} = (1 + \epsilon/2)\, C_g \cos\beta$ and $C_{gy} = (1 + \epsilon/2)\, C_g \sin\beta$ are components of the wave group velocity. The additional terms in eqns.(8) and (9) depend on angular resolution (through ϵ), group velocity and the spatial and angular inhomogeneity of the wave field.

2.2 A special case

Inclusion of the fifth term on the left-hand side of eq.(8) (or, equivalently, the last term of (9) in the plain surface case) in the energy balance equation of the WAM model would lead to substantial complications for the WAM numerical scheme. Calculation of the second-order derivatives would lead to a significant increase in required computation time. Under certain circumstances, however, it is possible to simplify the three contributions to the correction term considerably.

Let L be a typical scale length for wave propagation in the region of interest. For an ocean L will be in the order of several thousand kilometers, whereas for a shelf sea such as the North Sea L will typically be a few hundred kilometers. Following Booij and Holthuijsen [4], it can be shown that:

$$\frac{\partial(\overline{S}\,\cos\beta)}{\partial\phi} - \frac{1}{\cos\phi}\,\frac{\partial(\overline{S}\,\sin\beta)}{\partial\theta} \approx \frac{R}{L}\,\frac{\partial\overline{S}}{\partial\beta} \tag{10}$$

For a shelf sea, the factor (R/L) will be of the order of 10 or larger. Thus, the first two contributions to the angular correction term are likely to be an order of magnitude larger than the third, which was connected to the wave variance due to changes in β as the wave propagates along a great circle. By neglecting this third contribution, the energy balance equation is reduced to:

$$\frac{d\overline{S}}{dt} \approx \frac{\partial\overline{S}}{\partial t} + \frac{1}{\cos\phi}\,\frac{\partial}{\partial\phi}(\dot{\phi}\,\cos\phi\,\overline{S}) + \frac{\partial}{\partial\theta}(\dot{\theta}\,\overline{S}) + \frac{\partial}{\partial\beta}(\dot{\beta}\,\overline{S}) \approx A\,\frac{\epsilon C_g}{R}\,\frac{\partial^2\overline{S}}{\partial\beta^2} \tag{11}$$

where $A = R/L$. In other words, the terms correcting the energy balance equation for the finite width of the angular bands may be approximated by a simple diffusive operator, which describes a slight "exchange" of energy between the nearest angular components. The main problem with the solution of eq.(11) is associated with an accurate determination of the dimensionless parameter A. A large value of A (strong angular smoothing) is able to wipe out all details of the angular distribution; with too small a value of A the garden sprinkler effect will not be diminished.

For swell propagation on oceanic scales, A is of the order of 1-10. In this case, neglect of the $\partial^2 S/\partial\beta^2$-term is perhaps not justifiable, and the approximation of the energy balance

equation (1) by equation (11) may not be appropriate.

To obtain more insight in the behaviour of the solution of (11), let us consider the simpler but similar case of the heat equation with the same right hand side:

$$\frac{\partial \overline{S}}{\partial \tau} = \delta \frac{\partial^2 \overline{S}}{\partial \beta^2} \tag{12}$$

where

$$\delta = A\,(\Delta\beta)^2\, C_g/12R \tag{13}$$

The only non-trivial solution of (12) which is periodical in β is given by:

$$S_m(\beta,\tau) = B(m)\,\exp(\pm im\beta - m^2\tau\,\delta) \tag{14}$$

Here $B(m)$ is an arbitrary function of a constant m, which is defined by the initial conditions of the problem. In the course of time solution (14) relaxes to an isotropic spectrum:

$$\lim_{\tau\to\infty} S(\beta,\tau) = B(m) = \frac{1}{2\pi}\int S(\beta,0)\,d\beta \tag{15}$$

The e-folding timescale on which this relaxation occurs is:

$$\Delta\tau \approx 1/(\delta m^2) = 12R/(m^2A(\Delta\beta)^2C_g) = 48\pi R/(m^2A(\Delta\beta)^2gT) \tag{16}$$

T being the mean wave period. Since in nature wave spectra starting from anisotropic initial conditions do not become quasi-isotropic in this manner, we may suppose that the validity of the approximation (11) is limited by the condition:

$$\Delta\tau \geq t_{max} \tag{17}$$

where t_{max} is the maximum duration of the wave propagation to be considered. This condition allows us to obtain an upper limit to, and second estimate of, the value of A:

$$A \leq 48\pi R/(m^2A(\Delta\beta)^2\, g\, T\, t_{max}) \tag{18}$$

For a mean wave period of 10 sec, an angular resolution $\Delta\beta = \pi/12$, m=5 and a maximum duration of 36 hours, for example, we find that $A \leq 10^2$.

2.3 The numerical algorithm

The numerical realization of applying the correction for a finite angular resolution is achieved by a simple finite differences approximation:

$$S^{n+1}(\omega_k, \beta_l) \;=\; \nu S^n(\omega_k, \beta_{l-1}) \;+\; (1-2\nu) S^n(\omega_k, \beta_l) \;+\; \nu S^n(\omega_k, \beta_{l+1}) \qquad (19)$$

where $\nu = A\ C_g\ \Delta t/12R$ and $A = R/L$ is a dimensionless parameter, the value of which depends on the area to be described by the model. From eq.(13) it can be shown that ν does not depend on the angular resolution $\Delta\beta$. Essentially, eq.(19) represents an angular smoothing of the wave spectrum, a slight exchange of energy between neighbouring angular spectral components, which is applied at every propagation time step.

One way to test the algorithm is to check whether the total wave energy is conserved. To estimate the energy exchange for all directions, the spectrum is integrated over all angles:

$$\frac{2\pi}{L}\sum_{l=1}^{L} S^{n+1}(\omega_k, \beta_l)\ \Delta\beta \;=\; \frac{2\pi}{L}\sum_{l=1}^{L}\{\epsilon S^n(\omega_k, \beta_{l-1}) \;+\; (1-2\epsilon) S^n(\omega_k, \beta_l) \;+\; \epsilon S^n(\omega_k, \beta_{l+1})\}\Delta\beta \qquad (20)$$

Since the spectrum $S(\omega_k, \beta_l)$ is a periodic function of direction β_l, it is possible to show that operation (19) conserves total energy:

$$\frac{2\pi}{L}\sum_{l=1}^{L} S^{n+1}(\omega_k, \beta_l)\ \Delta\beta \;=\; \frac{2\pi}{L}\sum_{l=1}^{L} S^n(\omega_k, \beta_l)\ \Delta\beta \qquad (21)$$

3 Numerical simulations of swell propagation

To compare the performance of the standard first-order propagation scheme of the WAM model with that of the modified algorithm outlined above, we will investigate the solution of the energy balance equation for the case of pure swell propagation on a spherical surface. For this particular situation, an analytical solution can be obtained, which can then be compared to both the standard and modified WAM propagation schemes.

3.1 Initial conditions and integral characteristics

The following test set-up has been defined. A rectangular grid is chosen, extending in longitude from -12.0° to 12.0° and in latitude from 51.0° to 75.0°. The grid consists of

25x49 points; the grid spacing is 0.5° in latitude and 1.0° in longitude, which approximately corresponds to a 55km distance between neighbouring points near the center of the grid. The region is supposed to consist of sea points only, of uniform depth (250m) and without currents.

An initial disturbance is assumed to propagate from the center of this grid towards the south; the initial angle of mean wave propagation β_o (measured counterclockwise from the parallel) thus is equal to -90°. The spectrum of the initial distribution is taken to have the following form:

$$S_o(\omega, \beta, \phi, \theta, t = 0) \;=\; S_o(\omega, \beta)\; F(\phi, \theta) \;=\; S_o(\omega) Q_o(\beta) F(\phi, \theta) \tag{22}$$

where $F(\phi, \theta)$ is a spatial spreading function and $S_o(\omega, \beta)$ is the initial spectrum.

The frequency-dependent part of the initial spectrum is described by:

$$S_o(\omega) = (n+1)\;\; m_o \;\; \frac{\omega_{max}^n}{\omega^{n+1}} \;\; \exp\,[-(\frac{n+1}{n})\;(\frac{\omega_{max}}{\omega})^n] \tag{23}$$

where m_o is the zeroth moment of the spectrum, ω_{max} is the frequency of the spectral maximum and n is a parameter indicating the width of the frequency spectrum. The angular distribution function $Q(\beta)$ is assumed to be of the form:

$$Q_o(\beta) = \begin{cases} \frac{8}{3\pi}\cos^4(\beta - \beta_o) & \text{if } \mid \beta - \beta_o \mid \,<\, \pi/2 \\ \\ 0 & \text{if } \mid \beta - \beta_o \mid \,>\, \pi/2 \end{cases} \tag{24}$$

For the spatial spreading function $F(\phi, \theta)$ we adopt a form suggested by Burgers et al. [7]:

$$F(\phi, \theta) = \exp(\frac{-2R}{L}\sqrt{(\theta - \theta_o)^2 + (\phi - \phi_o)^2}) \tag{25}$$

in which L is a scale parameter describing the extent of the spatial distribution. L is taken to be 150 km.

The normalized total energy of the travelling disturbance, $\Sigma(t)$, can be defined as:

$$\Sigma(t) = E(t)/E(t = 0) \tag{26}$$

where

$$E(t) = \iiint\int S(\omega, \beta, \phi, \theta, t)\ R^2 \cos\phi\ d\omega\ d\beta\ d\phi\ d\theta \tag{27}$$

A second integral quantity of interest is the spreading of the wave energy over the grid area in time. The spreading parameter Θ(t) is defined as the square root of the area containing the waves with significant wave height h greater than 1/3 of the maximum value of wave height at moment t:

$$\Theta(t) = \sqrt{T(t)/T(0)} \tag{28}$$

where

$$T(t) = \iint F(\phi, \theta, t)\ R^2 \cos\phi\ d\phi\ d\theta \tag{29}$$

and F(ϕ, θ) is Heaviside's function:

$$F(\phi, \theta) \ = \ F(h(\phi, \theta, t) - \frac{1}{3} h_{max}(t)) \tag{30}$$

Another integral parameter, the evolution of which is of interest, is the root mean square wave height error RMS_h over the whole area. This quantity has been defined as follows:

$$\mathrm{RMS}_h(t) \ = \ \sqrt{\sum_{i,j} err^2(\phi_i, \theta_j, t)/N} \tag{31}$$

where N is the total number of grid points and err is the normalized local wave height error:

$$err(t) \ = \ \frac{(h_{model}(\phi, \theta, t) \ - \ h_{anal}(\phi, \theta, t)}{h^{max}_{anal}(t)} \tag{32}$$

$h^{max}_{anal}(t)$ is the maximum value of the significant wave height of the analytical solution over the entire grid at time t.

The spatial distribution of significant wave height at t=0 is presented in figure 1a. The maximum wave height, taken to be 10m, is located at the center of the spatially symmetric disturbance, at coordinates ϕ_o=72° and θ_o=0°. The mean wave period is 15 sec. Starting from the initial conditions (22-25), we will study the evolution of the parameters h, Σ and Θ in time, as derived by the analytical solution, by the standard WAM model and by a version of WAM modified to incorporate angular diffusion.

3.2 The analytical solution for pure deep water propagation

In the absence of energy sources and/or sinks, the wave energy remains constant along the path of propagation:

$$S(\omega, \beta, \phi, \theta, t) = S_o(\omega_o, \beta_o, \phi_o, \theta_o) \tag{33}$$

To find the initial values $\omega_o, \beta_o, \phi_o$, and θ_o, one must solve the ray equations (2)-(4). In the case of deep water and in absence of currents, the frequency of travelling waves remains constant: $\omega_0 = \omega$, and wave packets move along the geodesics curve, which is the nearest distance between two points on the spherical earth surface. By using (2)-(4), the equation of propagation for a wave packet may be represented in the form:

$$\ddot{\phi} + \frac{1}{2}\dot{\theta}^2 \sin 2\theta = 0 \tag{34}$$

$$\ddot{\theta}\cos^2\phi - \dot{\theta}\sin 2\phi = 0 \tag{35}$$

The value of the propagation angle β can be found from the projection of the group velocity C_g on the parallel:

$$\cos\beta = \frac{\dot{\theta}}{\sqrt{\dot{\phi}^2 + \cos^2\phi\,\dot{\theta}^2}}\cos\phi = \frac{2\,\omega R}{g}\,\dot{\theta}\cos\phi \tag{36}$$

By separating variables, equations (35)-(36) can be integrated:

$$\phi = \arcsin\left(\sqrt{1-\alpha^2}\,\sin\left[\frac{g}{2\,\omega R}(t-t_o) + \arcsin\left(\frac{\sin\phi_o}{\sqrt{1-\alpha^2}}\right)\right]\right) \tag{37}$$

$$\theta = \theta_o + \arctan\left(\frac{\sin\phi}{\sqrt{(\cos^2\phi\,/\alpha^2)-1}}\right) - \arctan\left(\frac{\sin\phi_o}{\sqrt{(\cos^2\phi_0\,/\alpha^2)-1}}\right) \tag{38}$$

where $\alpha = \cos\phi_o \cos\beta_o$. The constant parameters in (38)-(39) are found from the initial conditions: $\phi = \phi_o, \theta = \theta_o$ at t=t_o. From (37) it can easily be shown that the following quantity is constant along the ray:

$$\cos\beta\cos\phi = \cos\beta_o\cos\phi_o \tag{39}$$

From this equality, the initial value of the propagation angle β_o at latitude ϕ_o can be derived when the value of the spectrum $S(\omega, \beta, \phi, \theta, t)$ is defined at latitude ϕ. The range of possible

β_o, ϕ_o is given by the condition:

$$| \cos \beta_o | = | \cos \beta \cos \phi \; / \; \cos \phi_o | \leq 1 \qquad (40)$$

Values of β_o, ϕ_o for which this condition does not hold denote the area where the wave cannot exist, i.e. the area of the wave's shadow.

The analytical solution of the problem can now be found by substituting eqns. (37)-(39) into eqn.(34).

3.3 Numerical results

Figs. 1b-1d show the analytical solution of the evolution in time of $h(\phi, \theta$,t), starting from the initial conditions (22)-(25); they represent the situation respectively 12, 24 and 48 hours after t=0. Fig.2 shows the numerical solution of this propagation problem as derived by the standard WAM propagation scheme, using 12 directions and 25 frequencies. In fig.2a the distribution of mean wave height at t=24h is presented; fig.2b. shows the normalized error *err* of the WAM solution with respect to the analytical one. The effects of limited angular resolution clearly show up in the spatial distribution of wave height, and in particular in the error map: too much energy is concentrated along the direction of propagation (positive errors of more than 40 %), and too little along other directions (negative errors of up to 30 %).

The wave height distribution in fig.2 represents one extreme case, in which the direction of wave propagation coincides exactly with one of the main directions recognized by the model. The other extreme is given by the situation in which the propagation direction lies on the borderline between two angular bins. In this case, the wave height and error distributions are of the form given in fig.3. The errors are of the same order as in fig.2, but the distributions are very different: the single-peaked initial wave distribution is broken up into two systems, propagating southwards along two of the basic model directions at an angle of 30 degrees to the initial propagation angle. In these two situations the errors caused by the garden sprinkler effect are maximal; generally, the situation will be something in between. In the remainder, we will consider only the situation in which the propagation

direction coincides with one of the model directions.

Increasing the number of directions should diminish the garden-sprinkler effect [8,10]. The same computations have therefore been repeated with the WAM model with the number of directions increased to 24. The resulting height and error distributions at t=24h are presented in fig.4. Inspection of the error distribution shows that increasing the number of directions does indeed significantly improve the agreement between the numerical model and the analytical solution. Local wave height errors are down to 20 %.

The same propagation problem has been solved with a modified version of the WAM propagation scheme including angular diffusion (eq.20). For a scale length of wave propagation of 300-400 km (a typical value for North Sea circumstances), the diffusion parameter A is $\sim$ 20. The larger A is, the stronger the angular diffusion becomes. To study the impact of varying A, computations have been carried out for the WAM model using 12 directions and three different values of A: A=19, 37.5 and 75. The resulting distributions of mean wave height and error are given in figs.5-7, respectively.

It is evident from figs.5-7 that the introduction of angular smoothing in the WAM propagation scheme significantly diminishes the garden sprinkler effect. Wave amplitudes deviate less from the analytical solution; local wave height errors are down to 20 % or less. This is comparable to the results obtained with WAM using 24 directions, at half the computational cost.

The evolution of the normalized total wave energy $\Sigma(t)$ and the spreading function $\Theta(t)$ in time, for the analytical solution and the WAM results described above, is shown in fig.8. The wave energy $\Sigma(t)$ steadily decreases in time due to the outward flux of energy through the boundaries of the region. The closest approximation to the analytical solution of $\Sigma(t)$ is obtained with the standard WAM scheme with 24 directions. The modified WAM schemes are slightly more diffusive *on the whole* than the standard WAM model; it should be stressed, however, that the *distribution* of the wave energy is far more accurate in the case of the modified WAM schemes, for all values of A, than for the standard (12 directions)

WAM scheme.

This can also be seen from the behaviour of the spreading parameter $\Theta(t)$. $\Theta(t)$ increases almost linearly during the first 15 hours (fig.8b). After reaching a maximum at $t \approx 30h$, $\Theta(t)$ diminishes due to the flow of energy through the boundaries. The closest approximation to the analytical solution of Θ is achieved by the WAM model using 12 directions and an angular smoothing with $A = 19$. Thus, for this integral parameter, angular smoothing, which is accomplished at a minimal increase in computing time, gives better results than a doubling of the angular resolution.

As can be seen from fig.8b, the application of angular smoothing increases the degree of spatial spreading. Due to this fact, the energy flux through the boundary becomes larger and the total energy remaining in the area becomes smaller than in a situation without angular smoothing. This effect is evident in fig.8a; however, the impact on the total wave energy is fairly small.

The evolution of the root mean square error RMS_h in time is presented in fig.8c. For $t<12h$ the differences between the various numerical schemes are negligible. For $12<t<48h$, however, results deviate considerably. The RMS error is lowest in the case of the standard WAM propagation scheme using 24 directions (an overall error of $\leq 9\%$) and highest for the standard WAM model with 12 directions (an error of up to 20%). The improvements caused by the introduction of angular smoothing are obvious. For up to $t=\sim 30$ hours, the accuracy of the modified WAM scheme using 12 directions and an angular smoothing parameter $A = 37.5$ is comparable to that of the standard WAM scheme with 24 directions; only for larger durations of the propagation, the standard algorithm with 24 directions is clearly superior.

In order to test to what extent the results presented here were affected by the specific choice of the initial spatial distribution (equation 25), the above calculations were repeated for several other distribution functions of various shape and extent. Qualitatively, the resulting wave height distributions and error maps were very similar to the solutions

presented in figs.1-8, so we will not show them here. The anisotropy of the wave height distribution due to the limited angular resolution was strongest in the case of initial disturbances of small spatial extent; wave height errors in the direction of propagation could then reach levels of 70% or more.

4 Conclusions

1. Spectral wave models generally suffer from the so-called "garden sprinkler" effect, which is related to the angular discretization applied in the model. In the present paper a method of diminishing the garden sprinkler effect is proposed. An additional term to the discretized energy balance equation is derived, which corrects for the finite angular band width applied in the discretization of the spectrum. The advantage of using this correction term, in comparison with the similar approach followed by [4], is that it is defined locally and does not require the calculation of large scale parameters; it does however necessitate the computation of several additional higher order derivatives.

2. It is shown that for wave propagation over relatively small distances (several hundreds of kilometers) the correction term may be approximated by a more simple angular diffusive operator. Implementation of this operator in a spectral model tends to smoothen the spatial distribution of wave height. It is shown that modifying the spectral WAM model according to this approach leads to a substantial reduction of the garden sprinkler effect, while requiring a minimal additional amount of computation time.

3. A comparison between the modified WAM model, the standard WAM model and an exact analytical solution show that the modified WAM model using 12 directions gives results of an accuracy similar to that of the standard WAM model with 24 directions.

References:

1. The SWAMP group - "An intercomparison study of wind wave prediction models, Part 1: Principal results and Conclusions" - *Ocean wave modelling*, Plenum press, New York, 1985.
2. I. Isozaki and T. Uji - "Numerical modelling of wind waves" - *Jap. Meteor. Geoph.* **24**, 2, 207 (1973)
3. D.T.Resio, A.W. Garcia, C.L. Vincent - "A numerical study of wind wave propagation" - *Proc. Symp "Coastal Zone"*, San Francisco, ASCE vol. III, ASCE New York 1978, p.2085
4. N. Booij and L.H. Holthuijsen - "Propagation of ocean waves in discrete spectral models" - *Journal of Comput. Phys.* **68**, p.307-326, 1987
5. The WAMDI group: S. Hasselmann, K. Hasselmann, E. Bauer, P.A.Em Janssen, G.J. Komen, L. Bertotti, P. Lionello, A. Guillaume, V.C. Cardone, J.A. Greenwood, M. Reistad, L. Zambresky, J.A. Ewing - "The WAM model - a third generation ocean wave prediction model" - *J. Phys. Oceanogr.* **12**, p.1775-1810, 1988
6. I.V. Lavrenov, J.R.A. Onvlee, V.K. Makin - "A comparison between the propagation schemes of the WAM model and the interpolation ray method" - *KNMI memo OO-92-20* (unpublished manuscript), 1992
7. Burgers, G., Makin, V.K., Quanduo, G., and De Las Heras, M., "Wave data assimilation for operational wave forecasting at the North Sea", - *Third International Workshop on Wave hindcasting and forecasting,* May 19-22 1992 Montreal, Environment Canada Ontario, p.202-209
8. Zambresky, L.F., "Results from a one year evaluation of the global WAM model", - *ECMWF Technical Report* **63**, ECMWF Reading, 1989
9. Guillaume, A., "Statistical tests for the comparison of surface gravity wave spectra with application to model validation" - *J. Atm. Ocean. Techn.* **7**, p.551, 1991
10. Tolman, H.L., "Effects of Numerics on the Physics in a Third-Generation Wind-Wave Model" - *J. Phys. Oceanogr.* **22**, 1095-1111, 1992

Figure captions:

Fig. 1: The spatial distribution of wave height for the analytical solution of pure propagation over deep water

1a - the spatial wave height distribution at t=0 hours

1b - the spatial wave height distribution at t=12 hours

1c - the spatial wave height distribution at t=24 hours

1d - the spatial wave height distribution at t=48 hours

Fig. 2: The WAM solution for the case of pure swell propagation using 12 directions

2a - the spatial wave height distribution at t=24 hours

2b - the distribution of wave height errors at t=24 hours

Fig. 3: The WAM solution for the case of pure swell propagation using 12 directions, with a direction grid shifted over $\Delta\beta/2$ (=15 degrees).

3a - the spatial wave height distribution at t=24 hours

3b - the distribution of wave height errors at t=24 hours

Fig. 4: The WAM solution for the case of pure swell propagation using 24 directions

4a - the spatial wave height distribution at t=24 hours

4b - the distribution of wave height errors at t=24 hours

Fig. 5: The evolution of the spatial distribution of mean wave height for $A = 19.$

5a - the spatial wave height distribution at t=24 hours

5b - the distribution of wave height errors at t=24 hours

Fig. 6: The evolution of the spatial distribution of mean wave height for $A = 37.5$

6a - the spatial wave height distribution at t=24 hours

6b - the distribution of wave height errors at t=24 hours

Fig. 7: The evolution of the spatial distribution of mean wave height for $A = 75.0$

7a - the spatial wave height distribution at t=24 hours

7b - the distribution of wave height errors at t=24 hours

Fig. 8: The evolution of the integral parameters

8a - The normalized total energy $\Sigma(t)$ as a function of time

8b - The spatial spreading function $\Theta(t)$ as a function of time

8c - The root mean square error $RMS_h(t)$ as a function of time

The various test cases are indicated by the following symbols:

x - analytical solution

$\triangle$ - standard WAM solution for 12 directions (A=0.0)

$\diamond$ - standard WAM solution for 24 directions (A=0.0)

o - WAM solution for 12 directions and a 15 degree shift in the direction grid (A=0.0)

$*$ - modified WAM solution for 12 directions and $A = 19$

$\star$ - modified WAM solution for 12 directions and $A = 75$

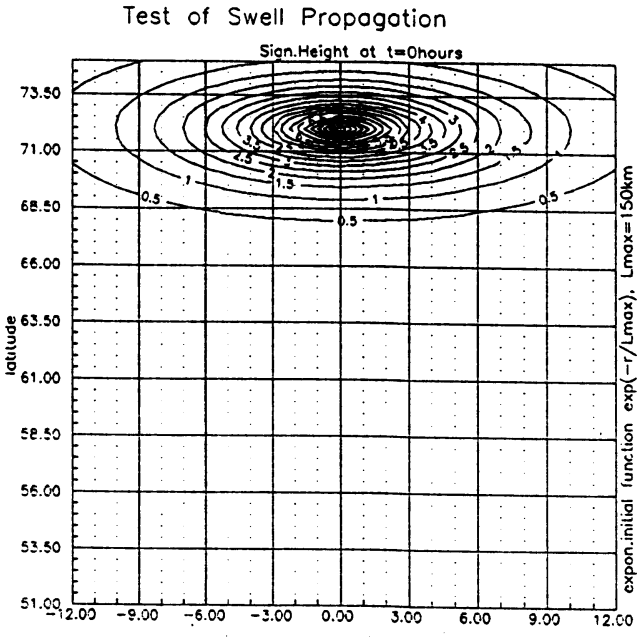

Fig.1a

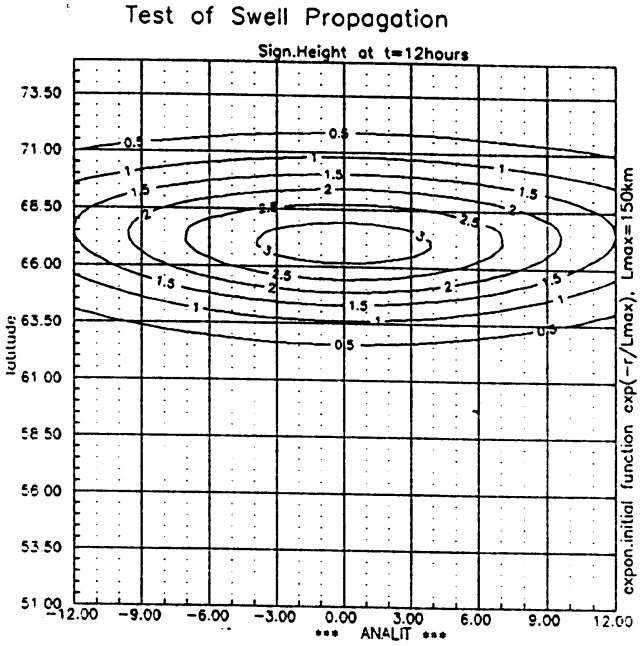

Fig.1b

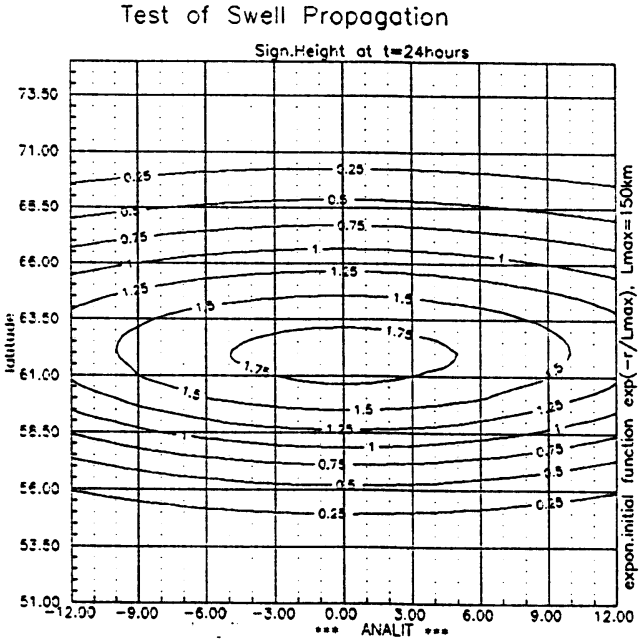

Fig.1c

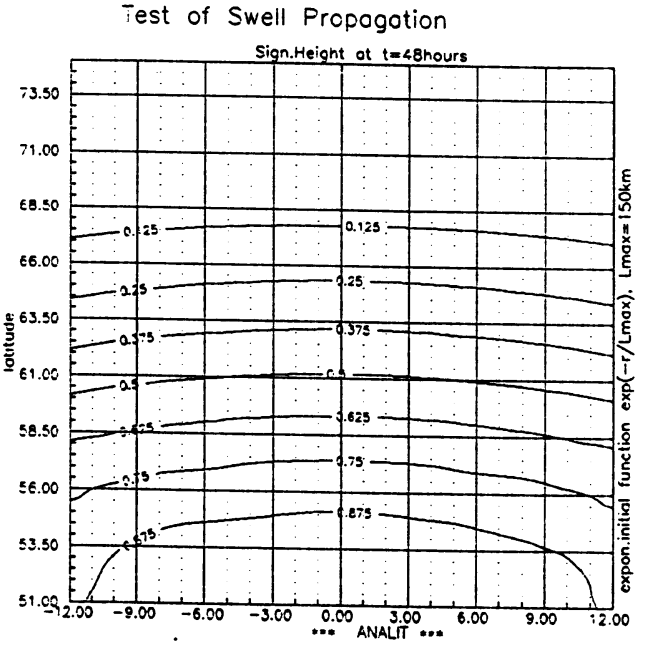

Fig.1d

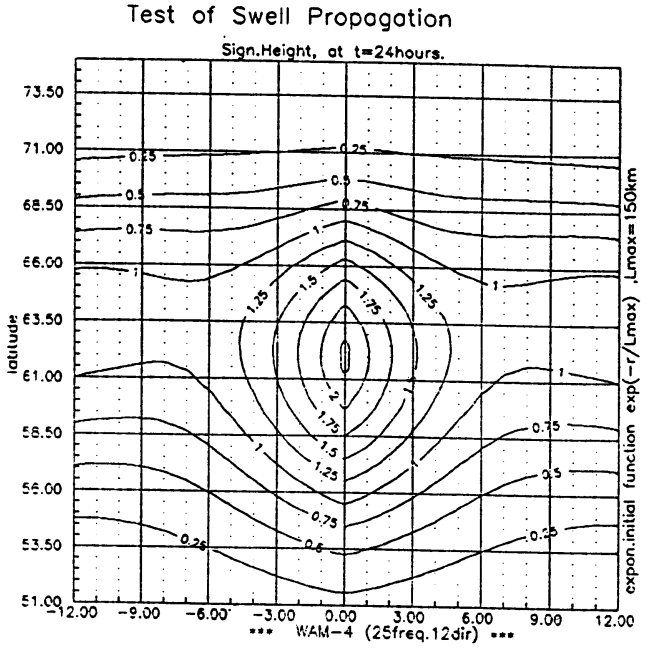

Fig.2a

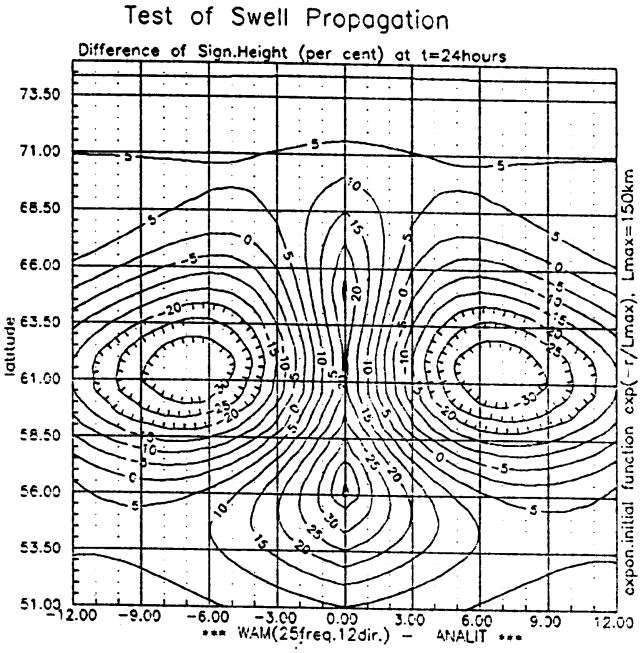

Fig.2b

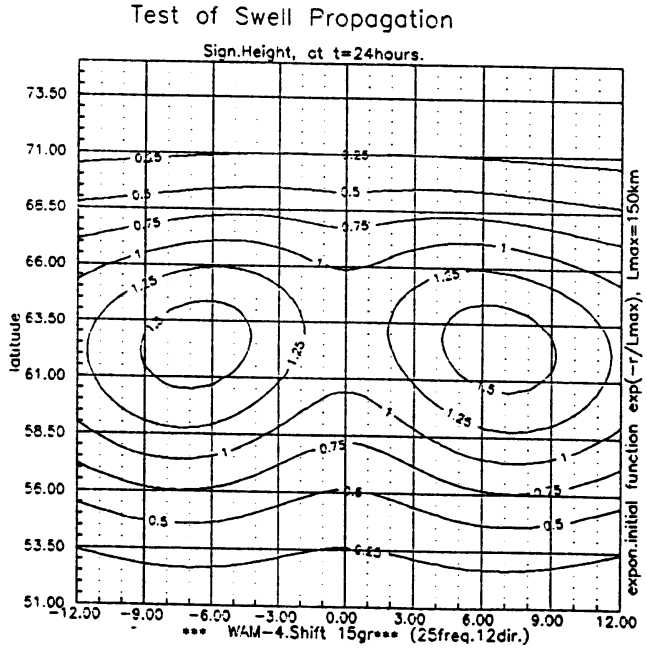

Fig.3a

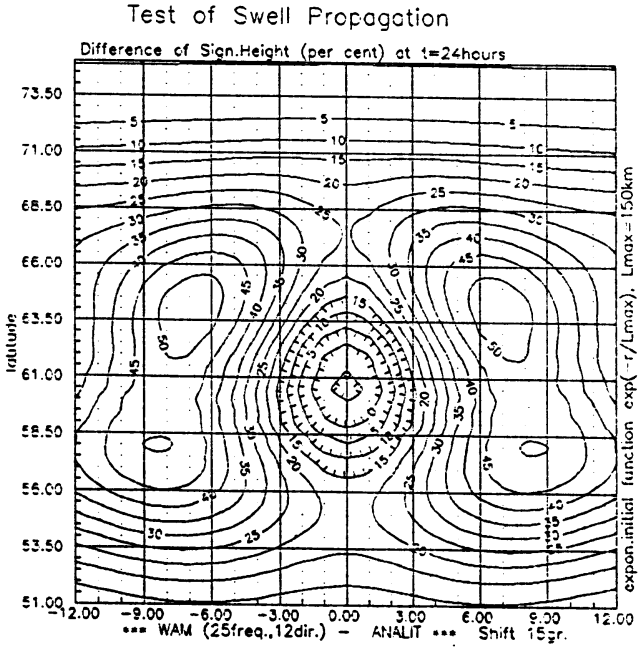

Fig.3b

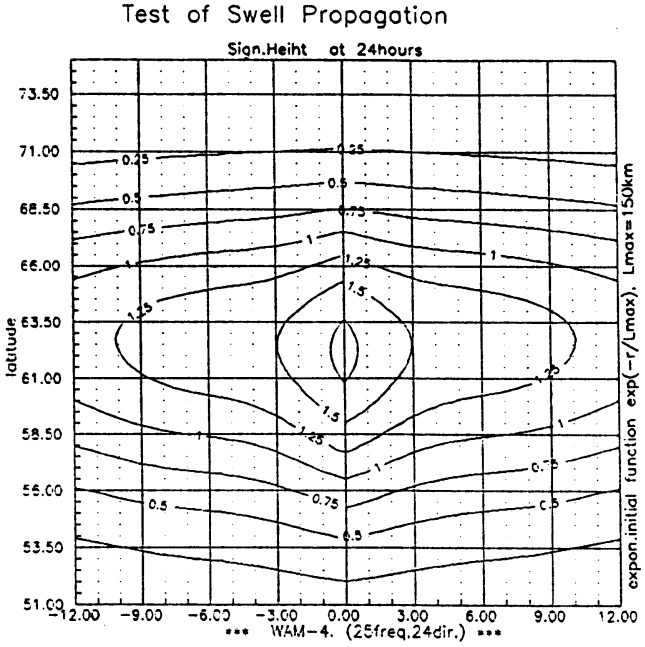

Fig.4a

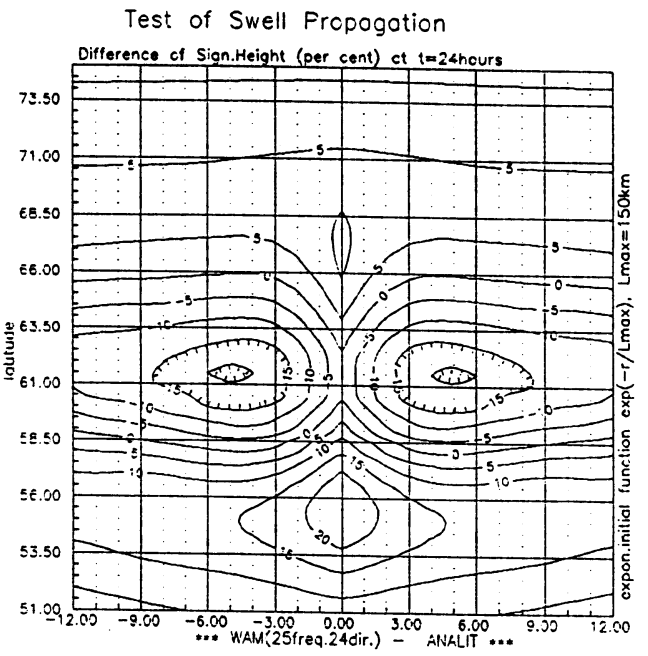

Fig.4b

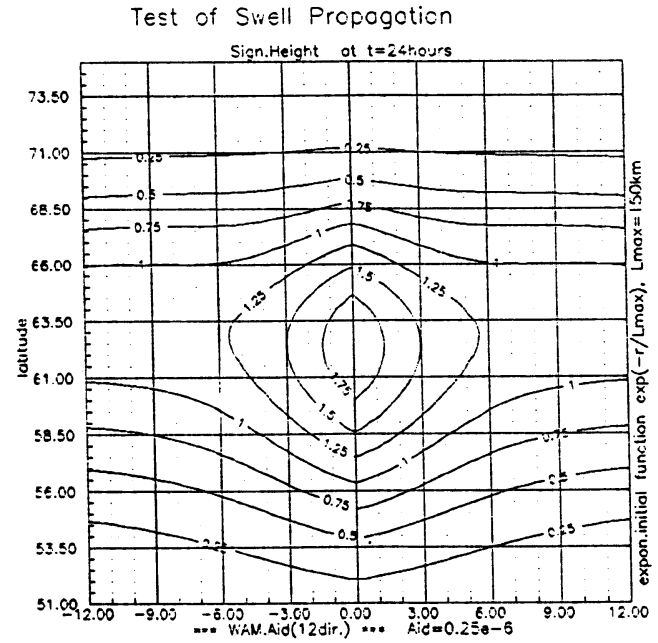

Fig.5a

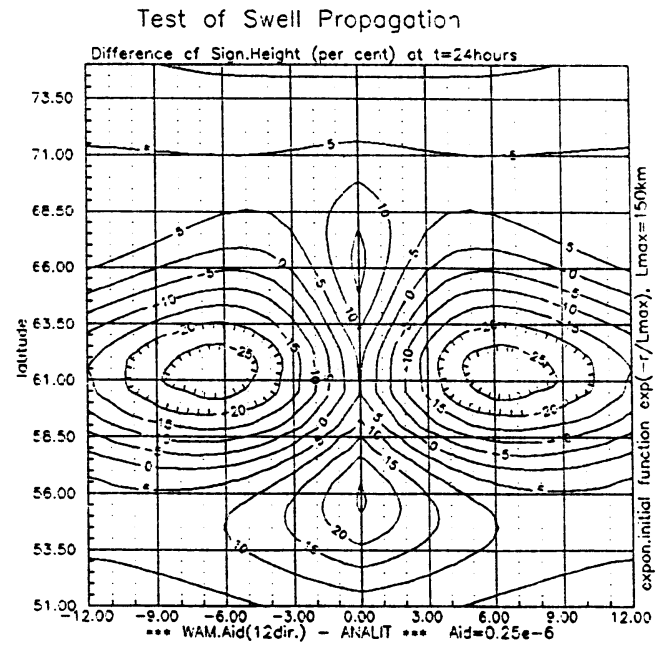

Fig.5b

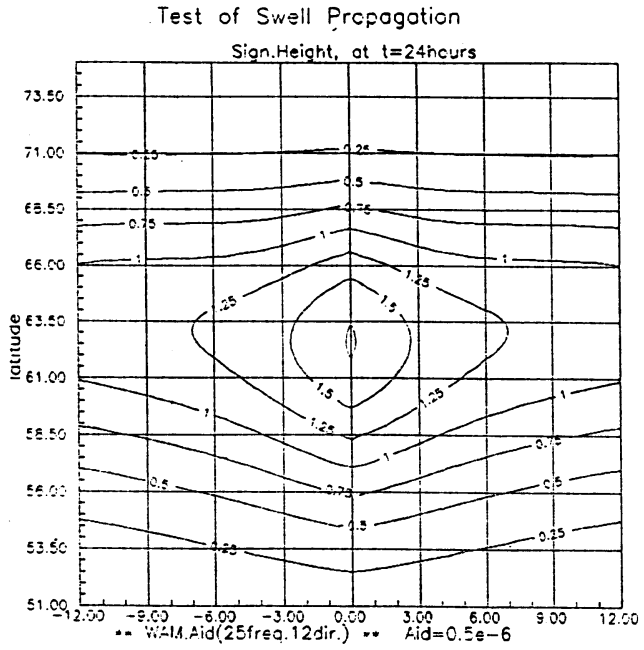

Fig.6a

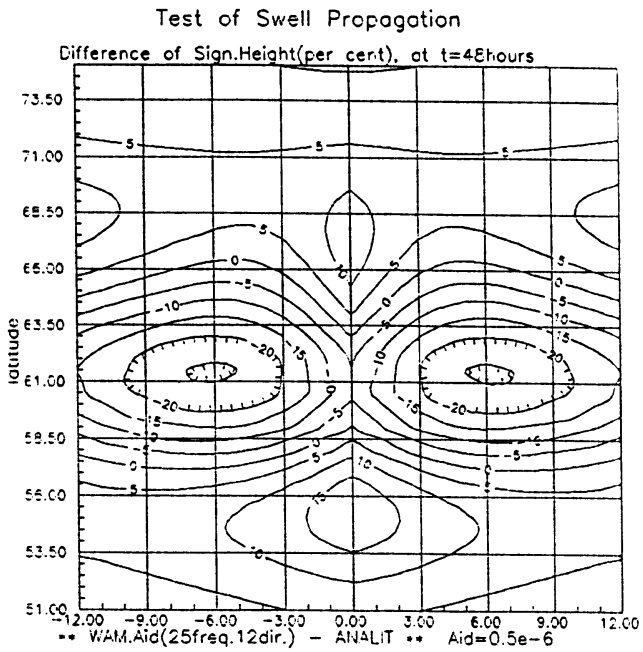

Fig.6b

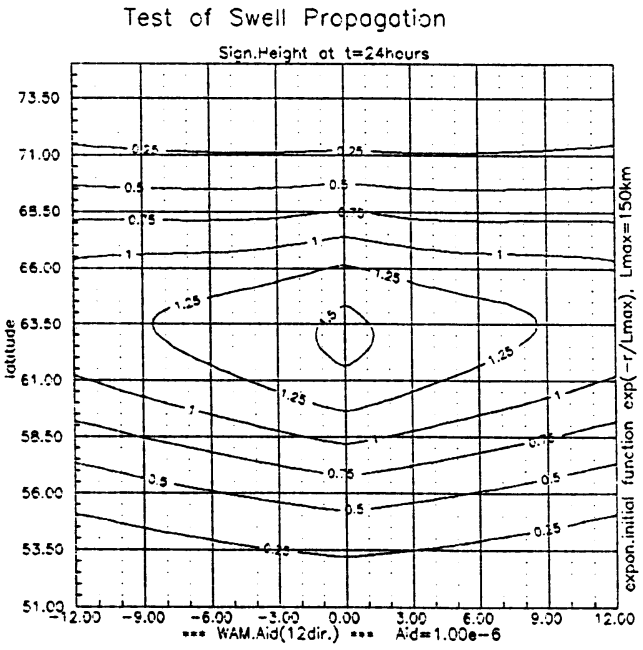

Fig.7a

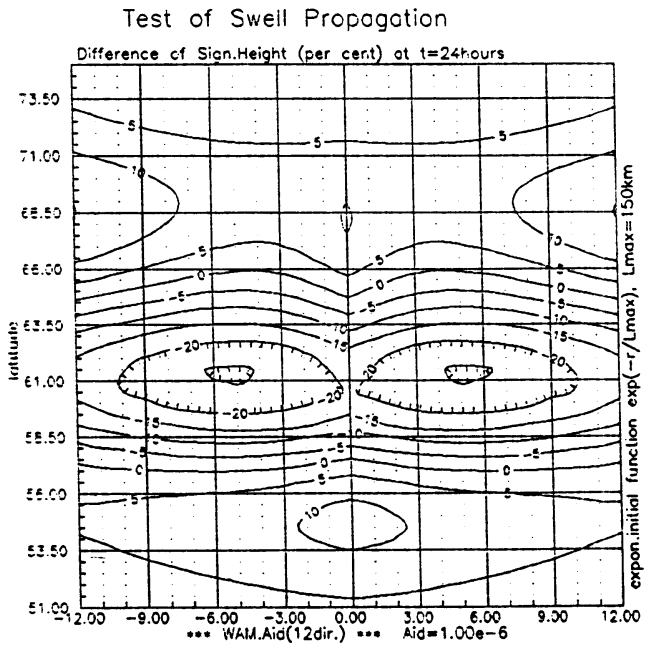

Fig.7b

THE TOTAL ENERGY

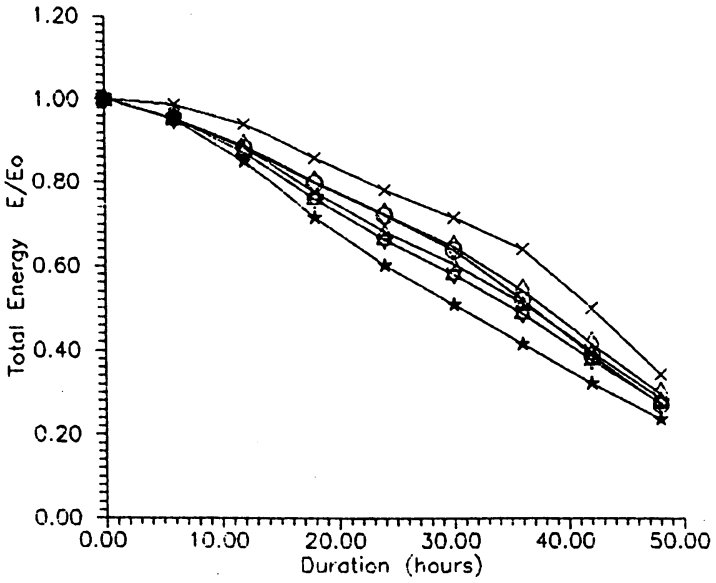

Fig.8a

Spatial Spreading Function

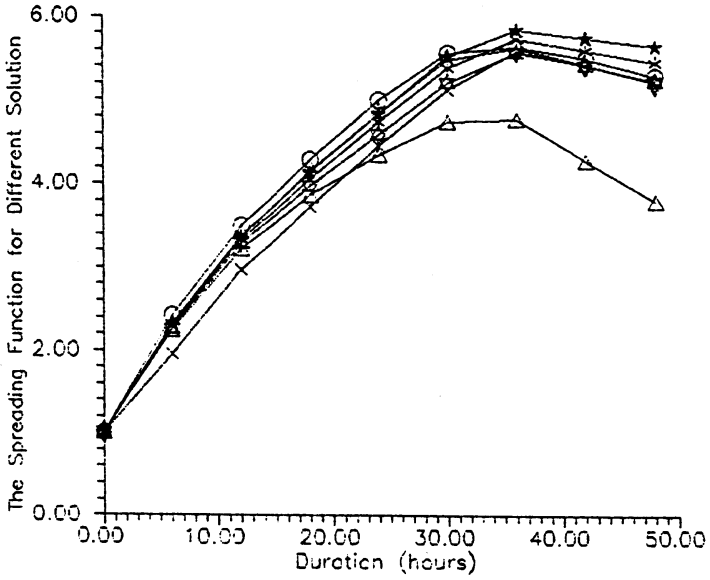

Fig.8b

The root mean square error

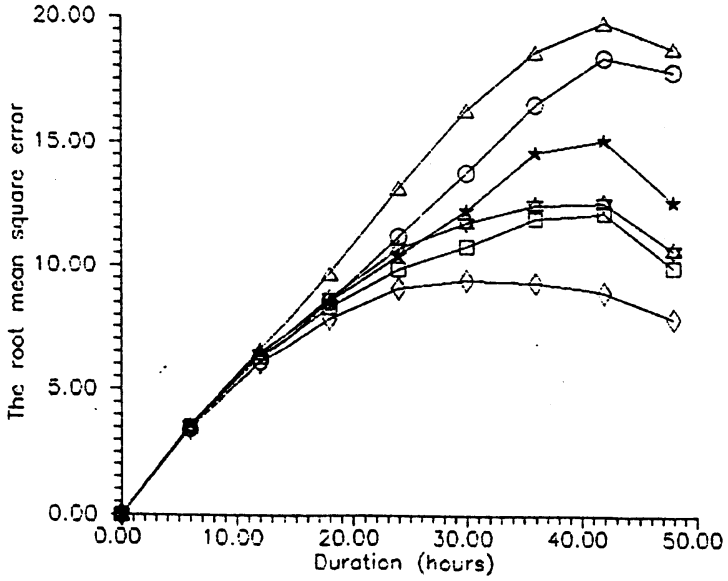

Fig.8c